2013 European Control Conference (ECC)
July 17-19, 2013, Zürich, Switzerland.

Improving Classification Performance through Kinematic Decisions

Weijia Zhang, Baro Hyun, Pierre Kabamba, Anouck Girard

Abstract— **We analyze the relationship between classification performance (i.e., the mutual information and the probability of misclassification) and sensor abilities. The analysis suggests an effective region of sensor space that can improve the classification performance when multiple measurements are to be taken sequentially, and possible sensor allocation strategies are discussed. Based on the analysis, we apply the sensing strategies to a UAV path planning problem where the sensor performance depends on the relative position (i.e., range and azimuth) of the UAV with respect to the object of interest. Specifically, we use two sliding mode controllers, each of which accounts for a particular sensing strategy, with a hybrid-system switching scheme. We validate our approach with numerical simulation results.**

I. Introduction

Unmanned Air Vehicles (UAVs) are used for Intelligence, Surveillance and Reconnaissance missions (ISR) in the U.S. Air Force [1]. UAVs collect data containing information about suspicious objects of interest and a decision is made as to whether the object of interest is a threat or not. This process is a binary classification.

A. Motivation

ISR missions involve information gathering and decision making. However, according to [2], "natural human capacities are becoming increasingly mismatched to the enormous data volumes, processing capabilities, and decision speeds that technologies either offer or demand."

One feature of UAVs is their ability to move in physical space, allowing more than one picture to be taken about the same object; however, as we will show, increasing the amount of information about an object may not improve classification performance. In this paper, we study strategies for path planning for UAVs and sensors using kinematic decisions that collect sufficient information about objects yet simultaneously improve classification performance.

B. Problem description

The problem is a simplified ISR mission scenario: a UAV is commanded to observe a geographic area which contains a non-moving object of interest. The UAV takes measurements to obtain more information and decides whether the object of interest is an enemy or not. The process can be treated as a binary classifier. We are interested in:

1) How to improve the classification performance by controlling sensor abilities.
2) If sensor abilities are related to the UAV's kinematic decisions, how to control the UAV trajectory to improve the classification performance.

The research was supported in part by the United States Air Force grant FA 8650-07-2-3744.

The authors are with the department of Aerospace Engineering, University of Michigan, Ann Arbor, MI 48109, USA {weijiaz, bhyun, kabamba, anouck}@umich.edu

C. Literature review and previous work

While the literature review portion has been reduced due to the space limits, a list of publications can be found in the Reference section [3], [4], [5]. [5], [6], [7],[6], [7], [8], [9], [10], [11].

In previous work, we have been investigating path planning problems with a particular interest in the coupling between decision-making (e.g., classification) and kinematic decisions of a mobile agent. Specifically, we posed the path planning problem as a constrained-optimization problem with various cost functions, such as Bayes risk [12], Shannon's mutual information [13], and the probability of error [14], where the optimizer is a sequence of kinematic decisions. In [15], we proposed a heuristic that returns a feasible solution to such an optimization problem.

D. Original contributions

The original contributions of this paper are as follows:

1) We analyze the relationship between classification performance and sensor abilities. The analysis suggests an effective region of sensor space that can improve the classification performance when multiple measurements are to be taken sequentially. Possible strategies for allocating sensor abilities are discussed.
2) Based on the analysis, we apply the sensing strategies to a UAV path planning problem where the sensor performance depends on the relative position (range and azimuth) of the UAV with respect to the object of interest. Specifically, we use two sliding mode controllers, each of which accounts for a particular sensing strategy, with a hybrid-system switching scheme. We validate our approach with numerical simulation results.

II. Theoretical background

1) Classifiers: A decider D is a deterministic mapping defined on a set of data into truth values, i.e.,

$$D : \{\text{data}\} \to \{T, F\}.$$

Processing of the data requires two abilities: recognizing truth out of truth (rate of true positives) and falsehood out of falsehood (rate of true negatives). These abilities are characterized by two independent parameters, σ_T and σ_F, respectively. Note that these parameters are entries in the confusion matrix in signal detection theory [16].

2) Probabilistic modeling: Let X be a discrete random variable that denotes the category of objects of interest that can take two realizations: either T or F.[1] There is a probability associated with the event that X be one of the realizations given as,

$$P(X=T)=u,\ P(X=F)=1-u, \tag{1}$$

where $u \in [0,\ 1]$. We denote u as the *prior probability* and it represents the proportion of T objects among the objects of interest.

The likelihood of the object property given the object category is modeled by conditional probabilities. For two-option object categories and two-option object properties, the conditional probabilities are given as,

$$\begin{aligned} &P(Y=Y_1|X=F)=\sigma_F,\ P(Y=Y_2|X=F)=1-\sigma_F,\\ &P(Y=Y_2|X=T)=\sigma_T,\ P(Y=Y_1|X=T)=1-\sigma_T, \end{aligned} \tag{2}$$

where $\sigma_F, \sigma_T \in [0.5,\ 1]$. 0.5 means pure guess and 1 means perfect sensor measurement.

3) Mutual information: Given two random variables (X and Y), Shannon's mutual information [3] describes the uncertainty reduction in one of the random variables (X) by observing another (Y), i.e.,

$$I(X;Y)=H(X)-H(X|Y), \tag{3}$$

The mutual information (I) and the probability of misclassification(P_m) can be expressed in terms of σ_T and σ_F (defined in Eq. (2)), and are given as:

$$\begin{aligned} I(X;Y) = &-u\log u-(1-u)\log(1-u)\\ &+(1-\sigma_T)u\log\left\{\frac{(1-\sigma_T)u}{(1-\sigma_T)u+\sigma_F(1-u)}\right\}\\ &+\sigma_F(1-u)\log\left\{\frac{\sigma_F(1-u)}{(1-\sigma_T)u+\sigma_F(1-u)}\right\}\\ &+\sigma_T u\log\left\{\frac{\sigma_T u}{\sigma_T u+(1-\sigma_F)(1-u)}\right\}\\ &+(1-\sigma_F)(1-u)\log\left\{\frac{(1-\sigma_F)(1-u)}{\sigma_T u+(1-\sigma_F)(1-u)}\right\}, \end{aligned} \tag{4}$$

4) Maximum likelihood classification: The maximum likelihood classification is a decision rule determined by a threshold applied on posterior probabilities. Let $O_s \in \{T,F\}$ be a decision variable that follows

$$O_s=\begin{cases} T & \text{if } \frac{P(X=T|Y=Y_j)}{P(X=F|Y=Y_j)}>1,\ j=1,2,\\ F & \text{if } \frac{P(X=T|Y=Y_j)}{P(X=F|Y=Y_j)}\le 1,\ j=1,2, \end{cases} \tag{5}$$

where Bayes' rule provides the posterior probability of X given Y.

5) Probability of misclassification: The probability of misclassification is the sum of the probabilities of the two faulty outcomes (i.e., false positives and false negatives):

$$P_m=P(O_s=T\wedge X=F)+P(O_s=F\wedge X=T). \tag{6}$$

Under some reasonable assumptions, P_m can be derived as a function of σ_T, σ_F, and u which is presented following equation. The derivation can be found in [17].

$$\begin{aligned} P_m = &\delta_T(f_2)(1-\sigma_F)(1-u)+\delta_T(f_1)\sigma_F(1-u)\\ &+\delta_F(f_2)\sigma_T u+\delta_F(f_1)(1-\sigma_T)u, \end{aligned} \tag{7}$$

respectively.[2]

III. Motivational analysis

In this section, we analyze the performance metrics (I andP_m) with respect to the sensor performance parameters (σ_T and σ_F) through numerical simulation. The simulation is performed under the following assumptions:

1) A single UAV and an non-moving object of interest are present in the given area.
2) The prior information is un-informative, i.e., $u=0.5$.
3) When multiple measurements are taken, they are taken *sequentially*, not as a batch.

The one measurement case is shown in Fig. 1(a). The solid curve lines represent the level of information and the solid straight lines represent the probability of misclassification. The abscissa is σ_T and the ordinate is σ_F. We call this 2-dimensional space the *sensor space*. Fig. 1(b) shows a detailed zoom of the contour region that was shown in Fig. 1(a). There are three markings on the contour (a triangle, a square, and a cross), each indicating a different level of I and P_m in Fig. 1(b).

Observation 1. In Fig. 1(b), beginning at the cross and following the probability of misclassification level curve towards the square, although the I has increased, the P_m remains constant ($P_m=0.25$, $I=0.19 \rightarrow P_m=0.25$, $I=0.2$).

Observation 2. In Fig. 1(b), beginning at the square and following the information level curve towards the triangle, although the I is constant, the P_m has increased ($P_m=0.25$, $I=0.2 \rightarrow P_m=0.27$, $I=0.2$).

These observations demonstrate that increasing the I does *not always* imply decreasing the P_m. We call this the *counter-intuitive phenomenon*.

Analysis to multiple measurements is shown in Fig. 2. We liberally choose the σ set for first measurement as [0.8, 0.8]. For the second measurement, we can vary the sensing abilities from 0.5 to 1. Fig. 3 shows the corresponding planar analysis as a function of the sensor performance parameters.

Observation 3. In Fig. 3, we find that if both sensor abilities dropped, the I increases and P_m stays the same as after the first measurement. We call this the increasing information

[1]Note that "T" and "F" can be interpreted as "True" and "False", respectively, or as "Threat" and "Friend". The subsequent theory does not require choosing an interpretation.

[2]The performance measures for multiple measurements are omitted from presenting due to their lengthy derivation and form. The derivation can be found in [14].

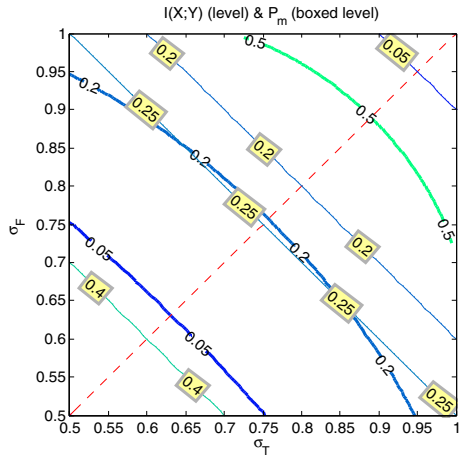

(a) Comparison of information and probability of misclassification

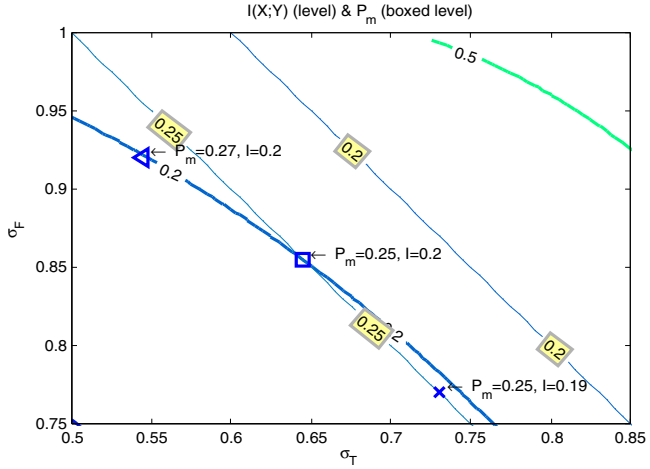

(b) Zoomed Fig. 1(a)

Fig. 1. Planar analysis for one-measurement case. The red dashed line is where $\sigma_T = \sigma_F$.

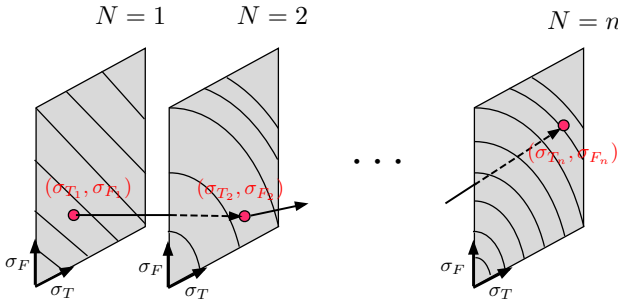

Fig. 2. Planar analysis concept for multiple measurements

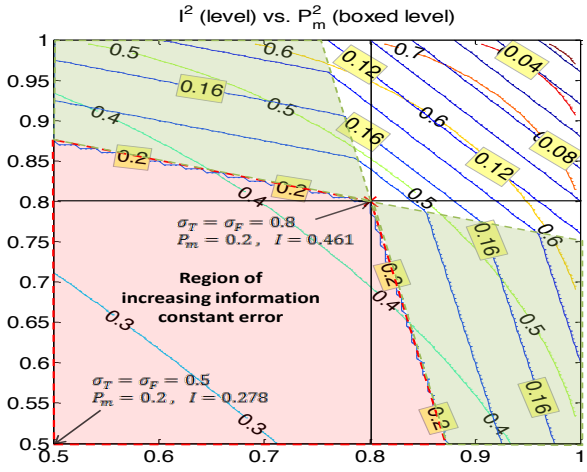

Fig. 3. Planar analysis of two-measurement case with $\sigma_T = \sigma_F = 0.8$

and constant error region, which is marked in red in the lower left corner of the figure.

Observation 4. In Fig. 3, the lower right and upper left corner are where one of the $\sigma_{(\cdot)}$ increased but the other one decreased. In these two regions, we find that the counter-intuitive phenomenon occurs only below two slanting tangent lines crossing at the initial point, which are marked in green. If the sensor abilities move close to these regions, it will be difficult to increase classification performance.

Note that if initial σ_T and σ_F are picked differently, the observations for both cases will still hold. The planar analysis suggests the following:

Rule 1. For the single measurement case, improving σ_T and σ_F simultaneously can prevent the counter-intuitive phenomenon.

Rule 2. For the two-measurement or multiple measurements cases, we can find a error-free region based on the priori probability and initial sensing abilities.

These two rules allow us to improve the classifier performance while collecting more information.

IV. Application to Path Planning Problem

In this section, we formulate and solve a path planning problem where we exploit the planar analysis results from the previous section. To formulate the problem, we utilize a simple unicycle model for the UAV kinematics and create a sensor model that depends on the relative position between the UAV and the object of interest.

A. Models

1) Kinematics: The UAV kinematics follow the unicycle model,

$$\begin{aligned} \dot{x} &= V\cos\psi, \\ \dot{y} &= V\sin\psi, \\ \dot{\psi} &= \mu, \end{aligned} \tag{8}$$

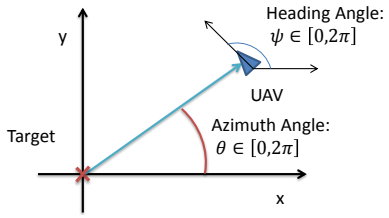

Fig. 4. Vehicle kinematics model

where $x \in \mathscr{R}$ and $y \in \mathscr{R}$ represent the position of the UAV with respect to the target-fixed frame (shown in Fig. 4), V is the velocity of the UAV, $\psi \in [0,\ 2\pi]$ is the heading angle, and μ is the control input. Since we assume that the velocity is constant, the only control input is the UAV turning rate μ.

2) Sensor: The sensor model assumes that the sensor performance depends on the relative position between the UAV and the object of interest, specifically, the performance degrades as the range between the two increases. Following our previous work [13], we use a sensor model that also accounts for the azimuth angle of the UAV, θ.

The sensor model can be broken down into two parts: range function and azimuth angle function. x and y are as in (13), the target is fixed at the origin and we assume that the sensor is always pointing to the target regardless the UAV heading angle. Two coefficients are introduced to characterize of the sensor: one is the range coefficient, denoted as $a \in \mathscr{R}$, and the other is the azimuth coefficient, denoted as $b \in [0,\ 1]$.

The range function depends on the distance from the UAV to the target. When the UAV moves within the range a, the range function is proportional to the relative distance. When the UAV gets closer and closer to the object within the focus range, the sensing ability decreases. We have the maximum sensing abilities at the focus range distance.
For σ_T, the range function $q_T(x,y)$ is:

$$q_T(x,y) = \begin{cases} \frac{\sqrt{(\frac{x}{2})^2+y^2}(1-b)}{a}+b & \text{if } \sqrt{(\frac{x}{2})^2+y^2} < a, \\ \frac{a(1-b)}{\sqrt{(\frac{x}{2})^2+y^2}}+b & \text{else.} \end{cases} \quad (9)$$

For σ_F, the range function $q_F(x,y)$ is:

$$q_F(x,y) = \begin{cases} \frac{\sqrt{(\frac{y}{2})^2+x^2}(1-b)}{a}+b & \text{if } \sqrt{(\frac{y}{2})^2+x^2} < a, \\ \frac{a(1-b)}{\sqrt{(\frac{y}{2})^2+x^2}}+b & \text{else.} \end{cases} \quad (10)$$

Let $\theta \in [0,\ 2\pi]$ be the azimuth of the UAV. The azimuth function $p(\theta)$ is the same for both σ,

$$p(\theta) \quad = \quad (1-\frac{b}{2})cos(\theta)+\frac{b}{2} \quad (11)$$

where $\theta = \arctan(\frac{y}{x})$.

The sensor function is the product of the range and the azimuth angle functions:

$$\begin{aligned} \sigma_T &= q_T(x,y)\cdot p(\theta), \\ \sigma_F &= q_F(x,y)\cdot p(\theta). \end{aligned} \quad (12)$$

Fig. 5 shows the contour plot for σ_T in the $x-y$ plane for $a = 10$ and $b = \sqrt{0.5}$. For σ_F, the contour plot is identical to that of σ_T, except for the orientation. Note in Fig. 5 that these two functions are symmetric for convenience. The sensing abilities can also be modeled based on other factors, such as shape of the target, environment, signal-to-noise ratio and power distribution.

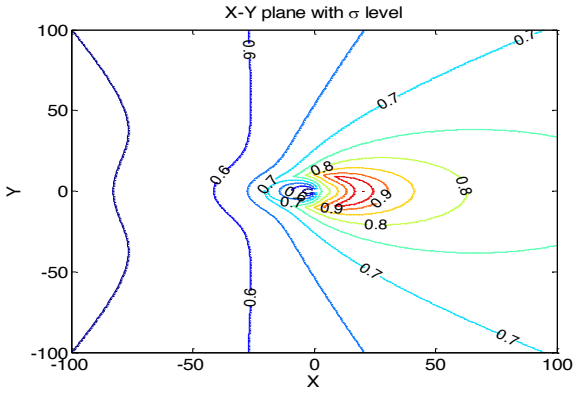

Fig. 5. σ_T contour plot in x-y plane

B. Problem formulation

Since the sensor abilities are functions of relative distances and azimuth angle, controlling the flight path results in changing sensor abilities. Given the UAV kinematic and sensing functions. the problem is to generate a consistent flight path, i.e., a flight path along which the amount of information increases and probability of misclassification decreases. We treat the sensor function as a manifold and apply sliding mode control [18] to solve the problem.

C. Sliding mode controller design

Assume the sensor model function is continuously differentiable and has the following form:

$$\sigma_i = g_i(x,y), \quad i \in \{T,F\}. \quad (13)$$

Taking the derivatives of the sensor functions, we obtain:

$$\begin{aligned} \dot{\sigma}_i &= \frac{\partial g_i}{\partial x}\dot{x}+\frac{\partial g_i}{\partial y}\dot{y}, \\ \ddot{\sigma}_i &= \frac{\partial^2 g_i}{\partial x^2}\dot{x}^2+2\frac{\partial^2 g_i}{\partial x \partial y}\dot{x}\dot{y}+\frac{\partial^2 g_i}{\partial y^2}\dot{y}^2+\frac{\partial g_i}{\partial x}\ddot{x}+\frac{\partial g_i}{\partial y}\ddot{y}. \end{aligned} \quad (14)$$

Given below are the sliding mode control derivations for approach and push modes, which are denoted as μ_a and μ_p, respectively.

1) Approach to the sliding surface: The goal is to equalize σ_T and σ_F. We start by defining σ_T and σ_F as state variable η and the desired state η_d, respectively:

$$\begin{aligned} \eta &= \sigma_T, \\ \eta_d &= \sigma_F. \end{aligned} \quad (15)$$

Let e be the error vector such that

$$e = \eta - \eta_d. \tag{16}$$

Selecting the sliding surface to be

$$S = \dot{e} + Ke, \tag{17}$$

Where K is a positive number.

If S goes to zero, we have exponentially decreasing error dynamics, at the rate set by K, a tuning parameter. Rewriting the equation for S, we have

$$S = \dot{\eta} - \dot{\eta}_d + Ke. \tag{18}$$

Taking the derivative of S,

$$\dot{S} \quad = \quad \ddot{e} + K\dot{e}. \tag{19}$$

Let the sliding surface be $\dot{S} = -\Lambda S$, where Λ is a positive number. Then we obtain the control input μ by manipulating the equation.

$$\ddot{\sigma_T} - \ddot{\sigma_F} + K(\dot{\sigma_T} - \dot{\sigma_F}) \quad = \quad -\Lambda(\dot{\sigma_T} - \dot{\sigma_F}) - \Lambda K(\sigma_T - \sigma_F)$$

Expanding the double derivative of σ_i, we obtain

$$\begin{aligned} &\mu_a(-(\tfrac{\partial g_T}{\partial x} - \tfrac{\partial g_F}{\partial x})V\sin(\psi) + (\tfrac{\partial g_T}{\partial y} - \tfrac{\partial g_F}{\partial y})V\cos(\psi)) \\ &= -(\Lambda + K)(\dot{\sigma_T} - \dot{\sigma_F}) - \Lambda K(\sigma_T - \sigma_F) - r_T + r_F. \end{aligned} \tag{20}$$

Solving for μ yields

$$\mu_a = \frac{-(\Lambda + K)(\dot{\sigma_T} - \dot{\sigma_F}) - \Lambda K(\sigma_T - \sigma_F) - r_T + r_F}{-(\frac{\partial g_T}{\partial x} - \frac{\partial g_F}{\partial x})V\sin(\psi) + (\frac{\partial g_T}{\partial y} - \frac{\partial g_F}{\partial y})V\cos(\psi)}. \tag{21}$$

This is the approach of the controller which attempts to achieve $\sigma_T = \sigma_F$. The next mode attempts to maximize both $\sigma_{(\cdot)}$.

2) Push towards the maximum: We want to control σ_i to reach maximum value. Starting from

$$\begin{aligned} \eta &= \sigma_T + \sigma_F, \\ \eta_d &= 2, \end{aligned} \tag{22}$$

we define e to be the error vector, and S to be the sliding surface as in the previous derivation. Again we let the sliding surface be $\dot{S} = -\Lambda S$, which yields the control input

$$\mu_p = \frac{-(\Lambda + K)(\dot{\sigma_T} + \dot{\sigma F}) - \Lambda K(\sigma_T + \sigma_F - 2) - r_T - r_F}{-(\frac{\partial g_T}{\partial x} + \frac{\partial g_F}{\partial x})V\sin(\psi) + (\frac{\partial g_T}{\partial y} + \frac{\partial g_F}{\partial y})V\cos(\psi)}. \tag{23}$$

D. Hybrid system design

Since our goal is to increase σ_T and σ_F simultaneously, two feedback control laws (21), (23) have to work together. To achieve this, we introduce a hybrid system for the UAV flight control where an error state $e = \sigma_T - \sigma_F$ provides the condition for switching modes. When the difference between the two $\sigma_{(\cdot)}$ is greater than a threshold, the system uses the approach feedback to place the UAV at a state that minimizes the difference. Fig. 6 shows the schematic view of the hybrid system.

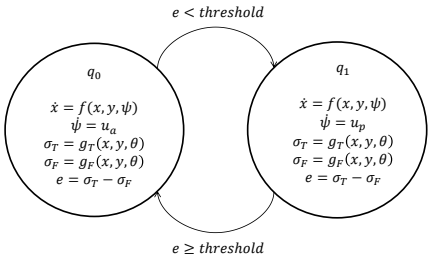

Fig. 6. Hybrid system for sliding mode control

V. Numerical simulation results

In this section, we present some numerical simulation results using the sliding mode controller with the hybrid switching law. The UAV has a constant speed of 1.3 *unit distance/sec* and a turn rate input limitation of 30 *deg/sec*. Initially, the UAV enters the suspicious area ([60 90] facing the target) and flies until $t = 40sec$ before taking the first measurement. For the single measurement case, we plot the $x-y$ position space in Fig. 7(a). Units of x and y are normalized distance units. Based on *Rule 1*, the controller pushes both $\sigma_{(\cdot)}$ to the maximum to avoid a false improvement in classification performance. Fig. 7(b) shows the trajectory in the sensor space. ($threshold = 0.2$ for hybrid system) Before any measurement is taken, Fig. 7(c) shows the mutual information and probability of misclassification and does not show the counter-intuitive phenomenon.

We assume that the UAV will take the first measurement instantly after 40 seconds, and continue to move 40 seconds as shown in Fig. 7(d), before the second measurement is taken.The flight plan for the second time interval is generated by the hybrid system and follows *Rule 2*. The σ_T and σ_F are updated and used to calculate the second measurement sensor space. Since we want to increase both $\sigma_{(\cdot)}$ before the second measurement, given the characteristics of the sensor function, the UAV will fly towards the object.

Hybrid system with 0.1 threshold keeps the trajectory within the effective region in the sensor space as shown in Fig. 7(e). In Fig. 7(d), we can see that the UAV is gradually moving toward the line where $\sigma_T = \sigma_F$. When it is within the sensor focus range to the object, it turns away from it while trying to stay close to the line. We successfully limit the $\sigma_{(\cdot)}$ such that there is no counter-intuitive phenomenon in Fig. 7(f), i.e., we are not decreasing I while increasing P_m. The difference between the two $\sigma_{(\cdot)}$ is limited by the system and inside the sensor space, the trajectory is within the upper right corner which is the region shown effective in the planar analysis. In Fig. 7(f), there is a discontinuity at $t = 40$ *sec*, because the UAV gains knowledge after the first measurement. Throughout the simulation, the controller successfully improves the classifier performance and collects more information.

VI. Conclusion & Future work

In this paper, we have investigated the relation between classification performance and kinematic decisions. Analysis

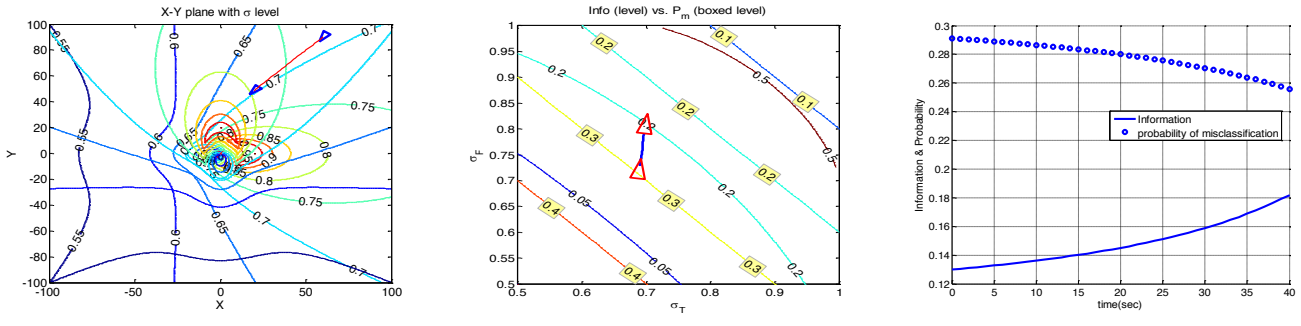

(a) One-measurement path in x-y space (b) Corresponding path in the ROC space (c) Corresponding performance metrics

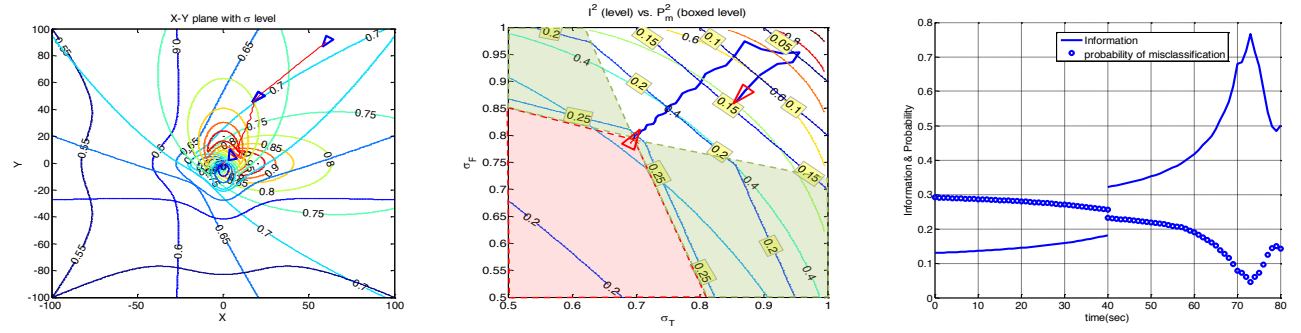

(d) Two-measurement path in x-y space (e) Corresponding path in the ROC space (f) Corresponding performance metrics

Fig. 7. Resulting paths by the sliding mode controller with hybrid switching scheme

showed that increasing I did not necessarily improve P_m and suggests two rules to avoid the phenomenon. Sensor abilities were introduced as functions of relative position and azimuth angle. Applied Sliding mode control for controlling sensor abilities in a path planning application. The results for this particular sensor function successfully showed both increasing information and improved classification performance.

In the future, the sensor function will be modified. It will may not necessarily only be related to the relative position and angle, e.g., sensor abilities can be based on properties of each object. Multiple-measurement case, geometric analysis in the sensing space and finding a mathematical representation of the effective region will be studied in the future.

REFERENCES

[1] Office of the Secretary of Defense. Unmanned systems integrated roadmap fy2011-2036. Technical report, 2011.

[2] United States Air Force Chief Scientist. Technology horizons a vision for air force science & technology, af/st-tr-10-01-pr. Technical report, 2010.

[3] C. Shannon. A mathematical theory of communication. *The Bell System Technical Journal*, (27:379–423, 623–656), 1948.

[4] R. Platt, R. Tedrake, L.P. Kaelbling, and T. Lozano-Perez. Belief space planning assuming maximum likelihood observations. In *Proceedings of Robotics: Science and Systems*, 2010.

[5] G. Zhang, S. Ferrari, and M. Qian. Information roadmap method for robotic sensor path planning. *Journal of Intelligent & Robotic Systems*, 56(1-2):69–98, 2009.

[6] R.C. Harney. Information-based approach to performance estimation and requirements allocation in multisensor fusion for target recognition. *Optical Engineering*, 36(3), Mar. 1997.

[7] J. Denzler and C.M. Brown. Information theoretic sensor data selection for active object recognition and state estimation. *IEEE Transactions on Pattern Analysis and Machine Intelligence*, 24(2):145–157, Feb. 2002.

[8] S.S. Gupta and L.-Y. Leu. On a classification problem: ranking and selection approach. Technical Report #89-27C, Department of Statistics, Purdue University, 1989.

[9] R.W. Holsapple, P.R. Chandler, J.J. Baker, A.R. Girard, and M. Pachter. Autonomous decision making with uncertainty for an urban intelligence, surveillance and reconnaissance (isr) scenario. In *Proceedings of AIAA Guidance, Navigation and Control Conference and Exhibit, Honolulu, HI, USA*, 2008.

[10] A.R. Girard, S. Dharba, M. Pachter, and P.R. Chandler. Stochastic dynamic programming for uncertainty handling in uav operations. In *Proceedings of the American Control Conference, New York City, NY, USA*, 2007.

[11] C. Kreucher, K. Kastella, and A. O. Hero. Sensor management using an active sensing approach. *Signal Processing*, 85:608–624, 2005.

[12] B. Hyun, P. Kabamba, W. Wang, and A. Girard. Sequential bayesian classification decisions for mobile sensors. In *Proceedings of IEEE Conference on Decision and Control, Atlanta, GA*, 2010.

[13] B. Hyun, P. Kabamba, and A. Girard. Optimally-informative path planning for dynamic bayesuab ckassification. *Optimization Letters*, 2011.

[14] M. Faied, P. Kabamba, B. Hyun, and A. Girard. Path planning for optimal classification. In *Proceedings of IEEE Conference on Decision and Control, Maui, HI*, 2012.

[15] Y. Chang, B. Hyun, and A.R. Girard. Path planning for information collection tasks using bond-energy algorithm. In *Proceedings of American Control Conference, Montreal, Canada*, 2012.

[16] L.L. Scharf. *Statistical signal processing (detection, estimation, and time series analysis)*. Addison-Wesley, 1991.

[17] B. Hyun, M. Faied, P. Kabamba, and A. Girard. Optimal classification by mixed-initiative nested thresholding. *IEEE Transactions on Systems, Man, and Cybernetics, Part A: Systems and Humans*, 2012. Under review.

[18] D. Swaroop, J.K. Hedrick, P.P. Yip, and J.C. Gerdes. Dynamic surface control for a class of nonlinear systems. *IEEE Transactions on Automatic Control*, 45(10):1893 – 1899, Oct. 2000.